AGU ADVANCING EARTH AND SPACE SCIENCE

Geophysical Research Letters

RESEARCH LETTER

10.1029/2021GL096009

Sector-Based Top-Down Estimates of NO_x, SO_2, and CO Emissions in East Asia

Zhen Qu[1,2], Daven K. Henze[1], Helen M. Worden[3], Zhe Jiang[4], Benjamin Gaubert[3], Nicolas Theys[5], and Wei Wang[6]

[1]Department of Mechanical Engineering, University of Colorado Boulder, Boulder, CO, USA, [2]School of Engineering and Applied Science, Harvard University, Cambridge, MA, USA, [3]Atmospheric Chemistry Observations and Modeling, National Center for Atmospheric Research, Boulder, CO, USA, [4]School of Earth and Space Sciences, University of Science and Technology of China, Hefei, China, [5]Belgian Institute for Space Aeronomy (BIRA-IASB), Brussels, Belgium, [6]China National Environmental Monitoring Center, Beijing, China

Key Points:

- A new sector-based multispecies inversion framework is developed to estimate NO_x, SO_2, and CO emissions using satellite observations
- The sector-based inversion leads to smaller biases and errors in surface NO_2 and SO_2 simulations than a species-based inversion
- The framework provides a new perspective to analyze the trend of emissions by sectors and evaluates bottom-up estimates

Supporting Information:

Supporting Information may be found in the online version of this article.

Correspondence to:

Z. Qu,
zhen.qu@colorado.edu

Citation:

Qu, Z., Henze, D. K., Worden, H. M., Jiang, Z., Gaubert, B., Theys, N., & Wang, W. (2022). Sector-based top-down estimates of NO_x, SO_2, and CO emissions in East Asia. *Geophysical Research Letters*, *49*, e2021GL096009. https://doi.org/10.1029/2021GL096009

Received 2 SEP 2021
Accepted 23 DEC 2021

Abstract

Top-down estimates using satellite data provide important information on the sources of air pollutants. We develop a sector-based 4D-Var framework based on the GEOS-Chem adjoint model to address the impacts of co-emissions and chemical interactions on top-down emission estimates. We apply OMI NO_2, OMI SO_2, and MOPITT CO observations to estimate NO_x, SO_2, and CO emissions in East Asia during 2005–2012. Posterior evaluations with surface measurements show reduced normalized mean bias (NMB) by 7% (NO_2)–15% (SO_2) and normalized mean square error (NMSE) by 8% (SO_2)–9% (NO_2) compared to a species-based inversion. This new inversion captures the peak years of Chinese SO_2 (2007) and NO_x (2011) emissions and attributes their drivers to industry and energy activities. The CO peak in 2007 in China is driven by residential and industry emissions. In India, the inversion attributes NO_x and SO_2 trends mostly to energy and CO trend to residential emissions.

Plain Language Summary

Satellite observations are widely used to estimate air pollutant emissions and evaluate their trends. We design a new method based on Bayesian statistics to estimate emissions of major air pollutants in East Asia according to their sources (e.g., energy, industry, transportation, etc.). Results from this approach show better agreement with independent surface measurements than the previous estimates that use observations to optimize emissions by species and estimates that compile emissions using activity data and emission factors. This method provides a new perspective to analyze the trend of air pollutants by sources and is crucial for countries and regions that lack detailed and timely emission estimates for each source sector.

1. Introduction

Nitrogen oxides ($NO_x = NO + NO_2$), sulfur dioxide (SO_2), and carbon monoxide (CO) are important air pollutants that affect atmospheric chemical processes and oxidative potentials (Seinfeld & Pandis, 2012). Anthropogenic SO_2 emissions mainly come from coal combustion in power plants; major sources of anthropogenic NO_x are from combustion in the transportation and energy sectors; CO emissions are mainly from incomplete combustion (Hoesly et al., 2018; McDuffie et al., 2020). Bottom-up methods estimate NO_x, SO_2, and CO emissions using activity rates and species emission factors, but these inventories have uncertainties of more than 100% and discrepancies of more than a factor of two at the national scale in Asia, especially for CO and in India (Elguindi et al., 2020; Hoesly et al., 2018; Kurokawa et al., 2013; Lu et al., 2011; McDuffie et al., 2020; Zhang et al., 2009; Zhao et al., 2011). Satellite observations have been applied to estimate pollutant emissions through inverse methods, including plume and box models (Beirle et al., 2011, 2019; Duncan et al., 2013; Fioletov et al., 2016, 2017; Goldberg et al., 2019; Li, McLinden, et al., 2017; Liu et al., 2018; McLinden et al., 2016), mass balance (Lamsal et al., 2011; Martin et al., 2003), 4D-Var (Jiang et al., 2015, 2017; Müller & Stavrakou, 2005; Qu et al., 2017; Qu, Henze, Li, et al., 2019; Wang et al., 2016), and Ensemble Kalman Filter (Ding et al., 2015; Gaubert et al., 2020; Miyazaki et al., 2012). Assimilations of observations of multiple species further improved inversion performance by accounting for the impacts of emission adjustments on the concentrations of unobserved species (Miyazaki et al., 2017; Qu, Henze, Theys, et al. (2019); Zhang et al., 2019).

10.1029/2021GL096009

In addition to species-based top-down estimates that adjust the total amount of emissions without differentiating their sources, observations of multiple species can assist the separation of emissions from different source sectors such as industry and transportation, since the ratios of CO to NO_x and CO to SO_2 are unique markers of emissions from different fuel types and combustion sources (Silva & Arellano, 2017; Tang et al., 2019). Optimizing emissions by sector provides valuable information regarding biases or mischaracterized trends in a specific activity, and therefore assists in correcting these emission inventories or interpreting atmospheric chemistry simulations that use these emission inputs. A sector-based inversion also more consistently adjusts emissions across species and provides a more natural framework for realistically characterizing the spatial correlations of emissions than species-based inversions. Sector-based inversions can be conducted using linear regression (de Foy & Schauer, 2019; Fioletov et al., 2021), spatial separation between regions dominated by different sources (Jeaglé et al., 2005), tracer correlations, or through a variational framework formulated with sector-specific activities as the variable parameter. The advantage of the last approach is the capability to separately evaluate emission factors and activity rates from the bottom-up inventory without externally specifying ratios of pollutants and chemistry regimes.

Here we develop a sector-based multispecies 4D-Var data assimilation framework and apply it to constrain the activity rates and species emission factors of NO_x, SO_2, and CO. This framework relates column densities to emissions and accounts for the uncertainties in observations and the biases of satellite retrievals at the various overpass times by comparing observations with concurrent simulations. We therefore are able to estimate the trends of sectoral emissions from anthropogenic and biomass burning sources in East Asia for the period 2005–2012. Due to expensive computational costs, we only perform inversions for each January of the 8 years, since natural emissions in January are relatively small compared to other months in East Asia.

2. Methods

2.1. Observations and Model

We use NO_2 and SO_2 observations from OMI and CO observations from MOPITT. OMI has a footprint of 13 × 24 km at the nadir and an overpass time of about 13:45 local time. We use the NASA standard product OMNO2 (Level 2, Version 3) tropospheric NO_2 slant column density (Krotkov et al., 2017) and the Royal Belgian Institute for Space Aeronomy (BIRA) SO_2 Level 2 product (Theys et al., 2015). We convert the simulated NO_2 and SO_2 mixing ratios to slant column densities using scattering weights following Qu et al. (2017); Qu, Henze, Li, et al. (2019); Qu, Henze, Theys, et al. (2019), and filter our data with low quality (see details in Supporting Information S1). CO vertical profiles are from the MOPITT Level 2 product Version 8 multispectral retrieval (Deeter et al., 2019). MOPITT has a footprint of 22 × 22 km and overpasses the equator at 10:30 local time. It provides global coverage every 3 days. Observations in both the thermal-infrared (TIR) and near-infrared (NIR) enable retrievals of CO vertical profiles (Worden et al., 2010). We assimilate the surface layer CO concentrations following Jiang et al. (2015) because it better represents surface emissions and is less affected by model transport errors.

We use monthly mean surface measurements of NO_2 and SO_2 concentrations over 669 sites from the China National Environmental Monitoring Center to evaluate the prior and posterior simulations in January 2010. The NO_2 measurements are made by a chemiluminescence analyzer with a molybdenum converter, which has interferences from NO_x oxidation products. We therefore apply a correction factor following Lamsal et al. (2008) to the simulated NO_2 to account for this impact in the evaluations. There are no national surface CO measurements available in China during the studied period. We average the measurements on a 0.5° × 0.667° grid, for a total of 248 grid cells.

The implementation of the sector-based inversion framework is based on the GEOS-Chem adjoint model (Henze et al., 2007) v35f. GEOS-Chem is driven by the Goddard Earth Observing System (GEOS-5) reanalysis meteorology field from the NASA Global Modeling and Assimilation Office (GMAO) (Bey et al., 2001). We perform nested-East Asia (70°−150°E, 0°–50°N) simulations at a horizontal resolution of 0.5° × 0.667° with dynamic boundary conditions from a global 4° × 5° simulation. The GEOS-Chem adjoint model includes the adjoint code for model processes of chemistry, transport, and wet and dry removal. It provides an efficient way to calculate the sensitivity of scalar functions of model variables (e.g., column densities and concentrations) to model parameters (e.g., emission scaling factors) (Henze et al., 2009; Kopacz et al., 2009).

GEOS-Chem uses a detailed O_x-NO_x-hydrocarbon chemical mechanism (Bey et al., 2001) and a sulfur cycle simulation based on the Goddard Global Ozone Chemistry Aerosol Radiation and Transport (GOCART) model (Chin et al., 2000). The concentration of OH and chemical losses of CO, NO_x, and SO_2 are simulated by the model. The gas and particle-phase partitioning is calculated through the aerosol thermodynamics scheme from Park et al. (2004). Dry deposition and wet deposition in GEOS-Chem follows Wesely (1989), Wang et al. (1998), and Liu et al. (2001). Anthropogenic emissions of NO_x, SO_2, NH_3, CO, NMVOCs, and primary aerosol are from HTAP (2010) inventory version 2 (Janssens-Maenhout et al., 2015). Three-hourly biomass burning emissions are from GFED4 (Giglio et al., 2013). Other nonanthropogenic emissions follow the setup in Qu, Henze, Theys, et al. (2019).

CO concentrations on January 1 of every year during 2005–2012 are adjusted to match MOPITT observations given the relatively long lifetime of CO and significant low biases of CO simulations (Barré et al., 2015; Fortems-Cheiney et al., 2011; Gaubert et al., 2016; Jiang et al., 2013; Kopacz et al., 2010; Zhang et al., 2019). We scale CO concentrations on January 1 by the ratio of averaged MOPITT and simulated CO column over the last week of December in the previous year and repeat the scaling to the resulting CO concentrations by applying the ratio in the first week of January in the inversion year. The global mean CO concentration at 0:00 GMT on January 1, 2010 increases by 34% and the error weighted difference between simulated CO and MOPITT observations reduces by 79% after the scaling.

2.2. Sector-Based 4D-Var Inversion

We implement weekly sector-based scaling factors for emissions of NO_x, SO_2, and CO. In the bottom-up inventory, emission of species l in sector k at a grid cell is expressed as:

$$E_{a,k,l} = A_{a,k} F_{a,k,l}, \tag{1}$$

where the subscript “a” stands for a priori, $A_{a,k}$ is the prior activity rate, $F_{a,k,l}$ is the prior emission factor, $E_{a,k,l}$ is the resulting prior emission. k ranges from 1 to 7 representing each of the seven sectors of transportation, industry, residential, aviation, shipping, energy, and biomass burning. l is the index for species.

Traditional top-down estimates optimize species scaling factors that are applied to the prior emissions as:

$$E_l = \sigma_l \sum_{k=1}^{7} A_{a,k} F_{a,k,l} = \sigma_l E_{a,l}, \tag{2}$$

where $E_{a,l}$ and E_l are the prior and posterior total emissions for species l. σ_l is the species emission scaling factor.

The cost function for an inversion using species scaling factors is

$$\begin{aligned} J_1(\sigma_{k,l}) = {} & \frac{1}{2} \sum_{c_N \in \Omega} (\boldsymbol{H}(\boldsymbol{c}_N) - \mathbf{SCD}_{obsN})^T \mathbf{S}_{obsN}^{-1} (\boldsymbol{H}(\boldsymbol{c}_N) - \mathbf{SCD}_{obsN}) \\ & + \frac{1}{2} \alpha \sum_{c_S \in \Omega} (\overline{\boldsymbol{H}(\boldsymbol{c}_S)} - \overline{\mathbf{SCD}_{obsS}})^T \overline{\mathbf{S}_{obsS}^{-1}} (\overline{\boldsymbol{H}(\boldsymbol{c}_S)} - \overline{\mathbf{SCD}_{obsS}}) \\ & + \frac{1}{2} \beta \sum_{c_C \in \Omega} (\boldsymbol{H}(\boldsymbol{c}_C) - \mathbf{VCD}_{obsC})^T \mathbf{S}_{obsC}^{-1} (\boldsymbol{H}(\boldsymbol{c}_C) - \boldsymbol{c}_{obsC}) \\ & + \frac{1}{2} \gamma_{r1} \sum_{l=1}^{3} (\boldsymbol{\sigma}_l - \boldsymbol{\sigma}_{a,l})^T \mathbf{S}_{a,l}^{-1} (\boldsymbol{\sigma}_l - \boldsymbol{\sigma}_{a,l}) \\ = {} & J_o + \frac{1}{2} \gamma_{r1} \sum_{l=1}^{3} (\boldsymbol{\sigma}_l - \boldsymbol{\sigma}_{a,l})^T \mathbf{S}_{a,l}^{-1} (\boldsymbol{\sigma}_l - \boldsymbol{\sigma}_{a,l}). \end{aligned} \tag{3}$$

$\mathcal{H}$ is the observation operator that maps species concentrations of NO_2 ($\boldsymbol{c}_N$), SO_2 ($\boldsymbol{c}_S$), and CO ($\boldsymbol{c}_C$) to observation space to be comparable with OMI NO_2 slant column density ($\mathbf{SCD}_{obsN}$), OMI SO_2 slant column density ($\mathbf{SCD}_{obsS}$), and surface CO concentration from MOPITT ($\boldsymbol{c}_{obsC}$). $\mathbf{S}_{obsS}$, $\mathbf{S}_{obsN}$, and $\mathbf{S}_{obsC}$ are the observation error covariance matrices, assumed to be uncorrelated, with retrieval uncertainties of NO_2, SO_2, and CO along the diagonal. We average monthly OMI ($\mathbf{SCD}_{obsS}$) and GEOS-Chem ($\mathcal{H}(\boldsymbol{c}_S)$) SO_2 SCDs overpassing each grid cell following Qu, Henze, Li, et al. (2019), Qu, Henze, Theys, et al. (2019). We scale SO_2 and CO prediction errors by α (the number of NO_2 observations to the number of grid cells that have SO_2 observations) and β (the number of NO_2 to CO observations) to weight all three observation terms equally in the cost function (Qu, Henze, Theys, et al. (2019)). Ω is the domain (in time and space) where observations are available.

$\mathbf{S}_{a,\,l}$ is the prior error covariance matrix for each species. The diagonal elements of $\mathbf{S}_{a,\,l}$ are estimated to be 0.4 for anthropogenic NO_x and SO_2, 1.0 for anthropogenic CO (Li, Zhang, et al., 2017), 0.2 for biomass burning SO_2, 1.4 for biomass burning NO_x, and 0.3 for biomass burning CO. These uncertainties are further adjusted by a regularization parameter, γ_{r1}, to balance model error and prior constraints. We chose $\gamma_{r1} = 100$ for January 2010, based on the minimization of total error (Henze et al., 2009), shown in Figure S1 in Supporting Information S1. $\boldsymbol{\sigma}_{a,l}$ is the vector of prior scaling factors and equal to 1. Off-diagonal error correlations are not specified given that emissions from different sectors have different correlation lengths.

For the sector-based inversion, we apply scaling factors σ_k to activity rates of all seven sectors from Equation 1, and $\sigma_{k,l}$ to the emission factors of NO_x, SO_2, and CO in transportation, industry, and residential sectors:

$$E_{k,l} = \sigma_k A_{a,k} \sigma_{m,l} F_{a,m,l}, \tag{4}$$

where k ranges from 1 to 7 representing the seven sectors in Equation 1, l ranges from 1 to 3 representing NO_x, SO_2, and CO, and m ranges from 1 to 3, representing transportation, industry, and residential sectors. Implementing spatially independent adjustments of emission factors provide more accurate quantifications of emissions (Li, Zhang, et al., 2017) and their trends. $\sigma_{m,l}$ corrects the errors in emission factors when one species is overestimated and another is underestimated in the same sector, in which the cost function cannot be reduced by simply adjusting the activity rates. Optimizing only these three sectors with the largest sensitivity to reduce the cost function avoids introducing more control parameters than the effective number of observations, which would lead to an under-constrained inverse problem and makes the algorithm harder to find solutions. There are 16 scaling factors ($7\ k + 3\ m \times 3$ l), 195,536 parameters (12,221 grid × 16 scaling factors), and 533,017 observations (436,286 NO_2 + 86,960 CO + 9,771 grids with SO_2 observations). However, we recognize that half of the observations are over the ocean and observations may not provide independent information from each other regarding emissions. The cost function in this framework is written as

$$\begin{aligned} J_2(\boldsymbol{\sigma}_k, \boldsymbol{\sigma}_{m,l}) = J_o + \gamma_{r2} \textstyle\sum_{k=1}^{7} (\boldsymbol{\sigma}_k - \boldsymbol{\sigma}_{a,k})^{T} \mathbf{S}_{a,k}^{-1} (\boldsymbol{\sigma}_k - \boldsymbol{\sigma}_{a,k}) \\ + \frac{1}{2}\gamma_{r2} \textstyle\sum_{m=1}^{3} \sum_{l=1}^{3} (\boldsymbol{\sigma}_{m,l} - \boldsymbol{\sigma}_{a,m,l})^{T} \mathbf{S}_{a,m,l}^{-1} (\boldsymbol{\sigma}_{m,l} - \boldsymbol{\sigma}_{a,m,l}), \end{aligned} \tag{5}$$

where $\boldsymbol{\sigma}_{a,k}$ and $\boldsymbol{\sigma}_{a,m,l}$ are the vectors of prior scaling factors and are equal to 1. $\mathbf{S}_{a,k}$ is the prior error covariance matrix of emission scaling factors for each sector, with their exponential decayed spatial correlation specified in the off-diagonal term. Based on the uncertainties from bottom-up emission inventories, we assume the diagonal elements of $\mathbf{S}_{a,k}$ to be 0.6 for transportation, 0.7 for industry, 1.1 for residential, 0.6 for aviation, 0.6 for shipping, 0.5 for energy (Kurokawa et al., 2013; Lu et al., 2011; Zhang et al., 2009), and 0.3 for biomass burning (Stibig et al., 2014) in the East Asia domain. The correlation lengths of the prior error covariance matrix are estimated based on the extent of land type coverage for biomass burning and the scales that activity rates for each anthropogenic sector in the MEIC inventory are collected. According to the bottom-up estimates, we use a value of 100 km for transportation (Zheng et al., 2014), 200 km for industry (Li, Zhang, et al., 2017; Streets et al., 2006), 200 km for residential (Saikawa et al., 2017), 100 km for aviation, 150 km for shipping, 0 km for energy (Li, Zhang, et al., 2017), and 200 km for biomass burning (Stibig et al., 2014). $\mathbf{S}_{a,m,l}$ is the prior error covariance matrix of $\boldsymbol{\sigma}_{m,l}$, which we assume to have the same correlation lengths as the corresponding sectors in $\mathbf{S}_{a,k}$. Following Kurokawa et al. (2013), the diagonal elements of $\mathbf{S}_{a,m,l}$ are 0.6 for industrial NO_x, 0.5 for industrial SO_2, 1.0 for residential NO_x, 0.6 for residential SO_2, 0.6 for transportation CO, 0.5 for transportation NO_x, and 0.4 for transportation SO_2. The inversion results are sensitive to the assumed uncertainties, which determine the extent to which emissions can be adjusted by the observations. We therefore reduce the uncertainties for residential and industrial CO from 1.7 (Kurokawa et al., 2013) to 1.1 and from 1.2 (Kurokawa et al., 2013) to 1.0 to avoid unrealistically small (i.e., zero) emissions in the posterior estimates. The correlation length affects how similar emission adjustments are in the adjacent grid cells. The regional scale inversion results are insensitive to the correlation length. We choose $\gamma_{r2} = 100$ for January 2010 (Figure S1 in Supporting Information S1). Regularization parameters in other years are scaled by the ratio of the number of NO_2 observations with those in January 2010 (Table S1 in Supporting Information S1).

10.1029/2021GL096009

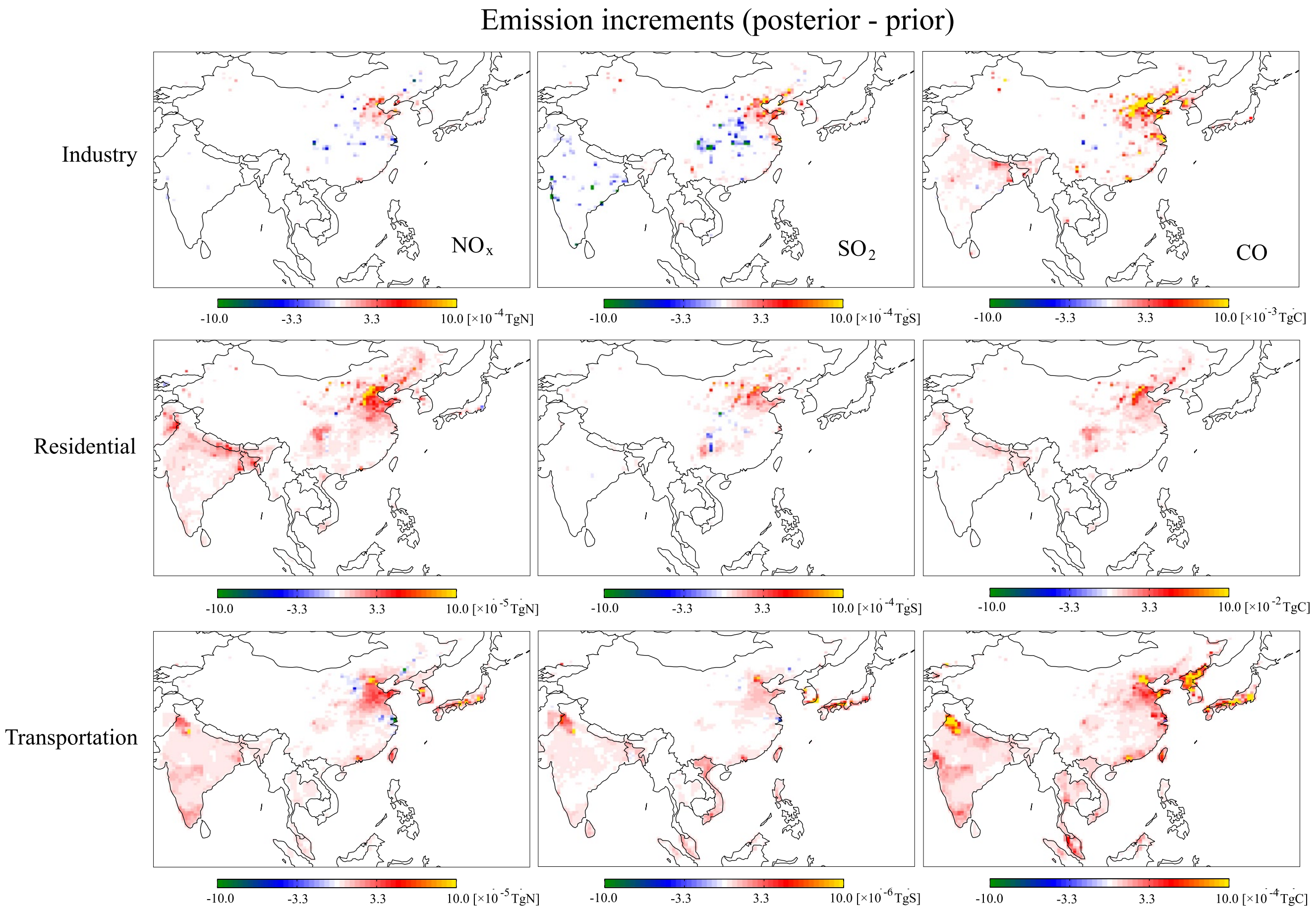

Figure 1. Sectoral emission increments in January 2010. We only show emissions from the industry, residential, and transportation sectors, which have the largest sensitivities to decrease the cost function.

3. Results

We average weekly posterior emissions over January in the following presentation to reduce random noise. Prior simulations underestimate NO_2 and CO by 30%–40% over North China Plain (NCP) and Guangdong province in January 2010 (see Figure S2 in Supporting Information S1). SO_2 simulations are mostly biased low north of 35°N by ~20% but are biased high by more than 50% south of 35°N. Posterior simulations reduced these biases and decrease the cost functions by 31% in the species-based inversion and 26% in the sector-based inversion, demonstrating the improved fit to observations.

Figure 1 shows the emission increments in the industry, residential, and transportation sectors in January 2010. The emission adjustments are in the same directions and have similar spatial patterns for all three species. Major corrections for NO_x and SO_2 emissions are from activity rates. Emissions in the North China Plain and Northeast China show large adjustments, consistent with the region of large adjustments from species-based inversions (Gaubert et al., 2020; Miyazaki et al., 2020; Qu, Henze, Theys, et al., 2019). The inversion suggests that the industry activity rates are underestimated by 5–15% in the HTAPv2 inventory over eastern China and central and northern India, but overestimated by less than 3% in the Sichuan and Shaanxi provinces of China. The residential activity rates are underestimated by more than 15% in HTAPv2 except for Tibet Plateau, southern India, southern Thailand, Cambodia, and central Vietnam. The transportation activity rates are underestimated by 10% in eastern China and central and northern India. The relatively consistent adjustments of sectoral emissions at the province (e.g., SO_2 in Shandong of China and residential emissions in Shandong and Hebei of China) or national level (e.g., CO in North Korea) can be explained by the relatively homogeneous emission factors and activity rates at these spatial scales (Li, Zhang, et al., 2017).

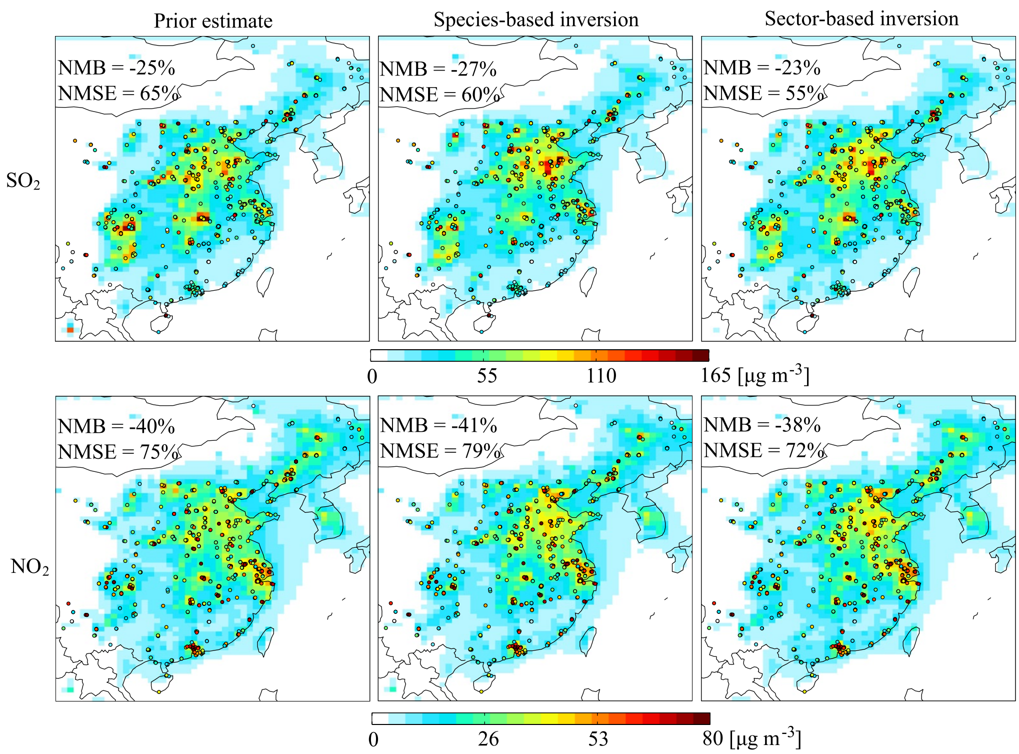

Figure 2. Monthly mean surface SO_2 and NO_2 concentrations from GEOS-Chem in January 2010. Correction factors are applied to the GEOS-Chem NO_2 simulations to account for the interference of NO_x oxidation products in the measurements. Surface measurements averaged over 248 grid cells are overlaid. The sector-based posterior simulations have the smallest normalized mean bias (NMB) and NMSE for both NO_2 and SO_2 when compared with surface measurements, shown inset.

Figure S3 in Supporting Information S1 shows the prior emissions summed over all sectors and their increments. Compared to the species-based inversion, the sector-based inversion shows smaller upward adjustments of NO_x and SO_2 emissions and larger upward adjustment of CO emissions over the North China Plain and larger downward adjustments of NO_x over India.

We focus on China and India in the following presentations since the inversion framework mainly optimizes anthropogenic emission sectors. Therefore, it is not ideal for regions where natural and background sources are significant (Qu et al., 2021; Silvern et al., 2019) and satellite retrievals have large uncertainties (Qu, Henze, Li, et al., 2019). On a national scale, all top-down NO_x emissions are smaller than the HTAPv2 emissions by 21–26% in China and 28% in India (Figure S4 in Supporting Information S1). Top-down SO_2 emissions are within 4% of the HTAPv2 estimates in China and are smaller by 39–61% in India, suggesting overestimates of bottom-up SO_2 emissions in India as pointed out by Qu, Henze, Li, et al. (2019) and Miyazaki et al. (2020). Top-down CO emissions are larger than the HTAPv2 estimates by 43–62% in China and 25–38% in India, and larger than the top-down estimates by Jiang et al. (2017) by 83–107% in China and 19–32% in India. The discrepancies in top-down CO estimates can be explained by the different assumptions of uncertainties in the bottom-up emissions, the inclusion of other chemical species in this study which adjusts OH fields (Qu, Henze, Theys, et al., 2019; Zhang et al., 2019), the use of surface layer CO concentrations instead of CO profiles (Jiang et al., 2013, 2017), and the different versions of MOPITT CO retrievals which cause up to 158% discrepancies in the CO budget over East Asia (Zhang et al., 2019).

The sector-based posterior simulations show larger surface NO_2 than the species-based one except for North China Plain, industrial regions in India, and parts of Myanmar and Cambodia; larger surface SO_2 except for Inner Mongolia, Shandong, Yangtze River Delta, and parts of Cambodia; and larger surface CO by up to 104% (Figure S5 in Supporting Information S1). Figures 2 and S6 in Supporting Information S1 show that the sector-based posterior simulations have the best agreement with the surface NO_2 and SO_2 measurements, although emission change alone does not significantly improve the model performance. The species-based posterior estimates have

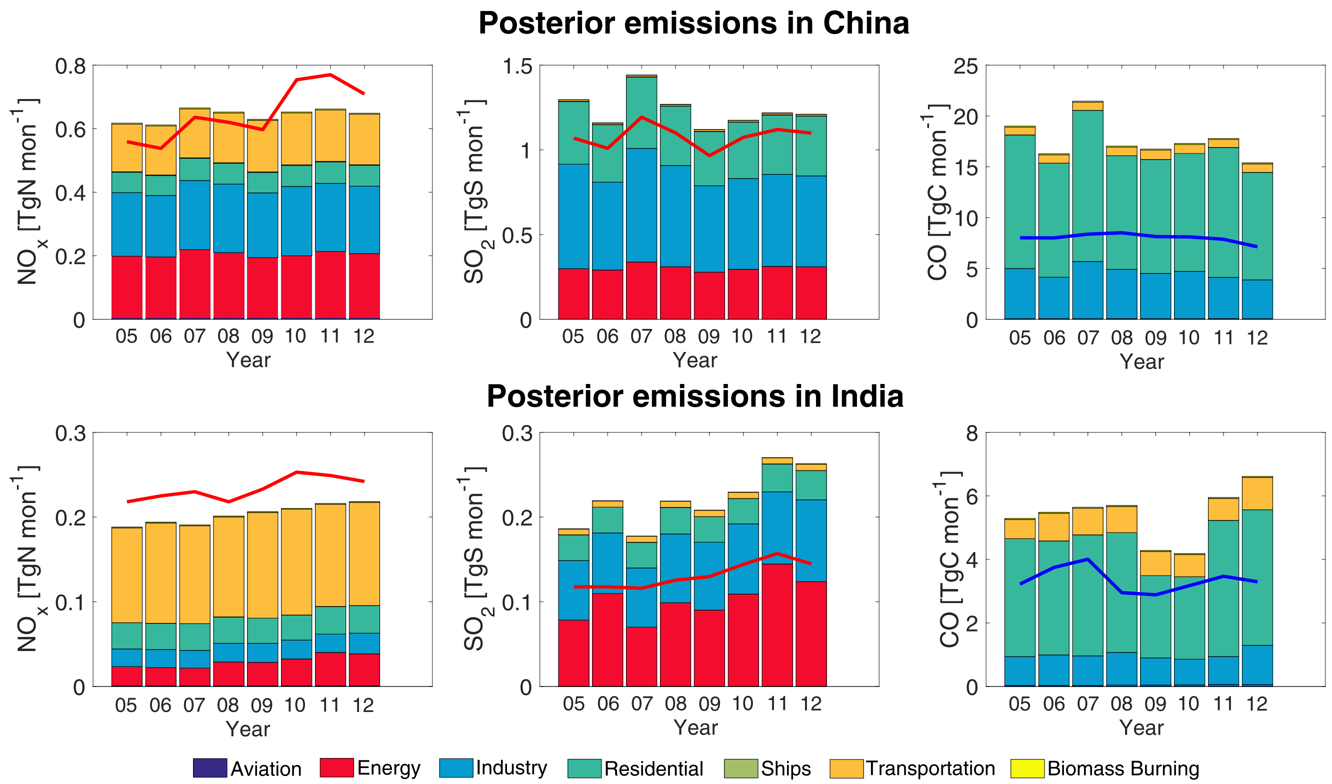

Figure 3. Top-down emissions in January 2005–2012 from the sector-based inversion. The red lines in the left and middle columns show species-based top-down estimates of all anthropogenic and natural emissions from Qu, Henze, Theys, et al. (2019). The blue lines in the right column show species-based top-down estimates of anthropogenic and biomass burning CO emissions from Jiang et al. (2017).

larger biases than the prior simulations due to the incorporation of CO observations and not considering their co-emissions—previous species-based inversion using only NO_2 and SO_2 observations show reduced bias for NO_2 (Qu, Henze, Theys, et al., 2019). The negative biases in NO_2 concentrations can be explained by the low bias of NO_2 satellite retrievals owing to the use of spatially coarse prior profiles (Laughner et al., 2016), uncertainties in NO_2 loss rate in the coarse resolution simulation (Valin et al., 2011), incapability to adjust emissions upward when NO_2 is below the satellite detection limit, and the lack of representation of the spatial gradients in NO_2 measurements in coarse resolution simulations (Qu et al., 2020). Following Qu et al. (2020), the resolution bias associated with averaging $0.1° \times 0.1°$ pseudo-NO_2 measurements to the $0.5° \times 0.667°$ grid is estimated to be 16%. Accounting for this reduces the NMB for prior and posterior simulations to −24%, −25% (species-based), and −22% (sector-based). Since the model grid cells are smaller than the smearing length scale of SO_2 (e.g., 260 km in the summer and 960 km in the winter using the definition of smearing length from Palmer et al., 2003 and SO_2 lifetimes from Lee et al., 2011), we expect small resolution bias in the comparison with SO_2 measurements. Posterior CO concentrations are larger than the prior simulations, consistent with previous top-down estimates (Gaubert et al., 2020; Miyazaki et al., 2020), but are hard to evaluate due to the lack of a national monitoring system over the studied period.

Figure 3 shows the trend of top-down emissions from the sector-based inversions in January 2005–2012. In China, these top-down NO_x emissions capture the trends from the species-based inversions in Qu, Henze, Theys, et al. (2019) before 2010. The changes in top-down NO_x emissions are mainly driven by the industry, energy, and transportation sector, which increased by 8%, 7%, and 8% from 2005 to 2011, consistent with the sectoral emissions from the bottom-up estimates in Liu et al. (2016). SO_2 emissions show the same peak in 2007 as the previous top-down estimates (Miyazaki et al., 2020; Qu, Henze, Li, et al., 2019; Qu, Henze, Theys, et al., 2019). Our estimates attribute this to the peak of emissions from the industry, energy, and residential sectors. The peak of SO_2 energy emission is consistent with the bottom-up MEIC estimates (Geng et al., 2017), but the peaks of industry and residential SO_2 emissions in 2007 are different from the continuous increase of the MEIC emissions. Since residential SO_2 emissions peak in January and is 3–4 times larger than emissions in April-October based on bottom-up estimates (Zheng et al., 2021), the trends and driving sectors for January are likely different from those for the whole year. CO emissions peak in 2007, consistent with previous top-down estimates (Jiang et al., 2017; Zheng et al., 2019), but differ from the continuous increase until 2008–2012 in the bottom-up estimates (Elguindi et al., 2020). CO emissions from the industrial and residential sectors decrease by 23% and 20% from 2005 to 2012, consistent with the reductions in annual bottom-up estimates in these two sectors in Zheng et al. (2018).

In India, the sector-based top-down emissions show consistent trends with the species-based top-down estimates from Qu, Henze, Theys, et al. (2019) and Jiang et al. (2017). Top-down emissions from the energy sector increase by 66% for NO_x and 58% for SO_2 and are the major driver of the increasing NO_x and SO_2 emissions in India. This is consistent with the 52% (NO_x) and 92% (SO_2) increases from 2005 to 2012 in the annual EDGARv5 bottom-up estimates (Crippa et al., 2020). Top-down CO emissions are driven by residential sources and fluctuate in India. However, bottom-up CO estimates from EDGARv5 show continuous increases in both the total and residential emissions.

4. Discussion and Conclusions

We apply a new sector-based 4D-Var inversion to estimate NO_x, SO_2, and CO emissions over East Asia using satellite NO_2, SO_2, and CO observations. Emission adjustments from the sector-based inversion are generally consistent with the species-based estimates in both magnitude and spatial distribution. The sector-based posterior simulations show better fits to the surface NO_2 and SO_2 measurements, demonstrating the more accurate emission estimates when incorporating constraints from co-emissions. Top-down estimates show that the increase of NO_x emissions until 2011 in China is driven by the industry, energy, and transportation sectors. Emissions from the industry, energy, and residential sector contribute to the peak of SO_2 emissions in 2007. The trend of China's CO emissions is driven by the decrease in residential and industrial emissions. In India, the continuous increase of NO_x and SO_2 emissions from 2005 to 2012 are mainly due to increase in the energy sector, and the fluctuations of CO emissions are driven by the residential sector. The sectoral contributions and trends from the top-down estimates are generally consistent with the bottom-up estimates except for CO emissions in India. Still, we recognize that sectors with large seasonal variations may show different emission adjustments and trends on an annual basis than the trends for January shown in this study.

We only perform the sector-based inversion for 1 month each year in this work due to the expensive computational cost (see details in Supporting Information S1). The trends of top-down emissions in January are generally consistent with previous yearly top-down estimates, but the sectoral breakdown may be different. Future development of inverse modeling frameworks based on chemical transport models with massively parallel architecture (e.g., Eastham et al., 2018) can expand the sector-based top-down estimates to multiple months and years.

Our estimates of CO emissions have the largest discrepancies compared to other top-down and bottom-up estimates. This is a well-known issue affected by model transport errors, uncertainties in OH fields, and different satellite retrievals (Arellano et al., 2004; Kopacz et al., 2010; Jiang et al., 2013, 2017; Müller et al., 2018; Yin et al., 2015; Zhang et al., 2019). In addition, the different biases and uncertainties of surface and column CO and the uncertainties assumed for prior emissions also affect top-down CO emission estimates. The lack of a monitoring network over the studied region and period hinders the validation of CO estimates. Still, incorporation of CO observations provides additional constraints on the sectoral attribution of emissions and ensures that the inverse problem is well-posed. Improvement in the accuracy of satellite retrievals, incorporation of other primary pollutants in the assimilation, and more detailed characterizations of the uncertainties in the bottom-up emission inventories have the potential to improve the sector-based emission estimates.

Data Availability Statement

The OMI NO_2 NASA product is downloaded from https://atrain.gesdisc.eosdis.nasa.gov/data/OMI/OMNO2_CPR.003/ (last access 1 September 2021). OMI SO_2 retrievals are from BIRA (http://sacs.aeronomie.be/products/product-details.php#omi, last access 1 September 2021). The MOPITT CO data are downloaded from https://search.earthdata.nasa.gov/search?q=mopitt (last access 1 September 2021). Surface measurements of NO_2 and SO_2 are obtained from CNEMC (http://www.cnemc.cn, only available in Chinese, last access 1 September 2021).

Acknowledgments

Z. Qu and D. K. Henze acknowledge funding support from National Aeronautics and Space Administration (NASA) NASA ACMAP NNX17AF63G. Z. Qu would also like to acknowledge high-performance computing support from Cheyenne (https://doi.org/10.5065/D6RX99HX) provided by NCAR's Computational and Information Systems Laboratory, sponsored by the National Science Foundation. The MOPITT and OMI projects are supported by the National Aeronautics and Space Administration (NASA) Earth Observing System (EOS) Program. Part of this work is supported by the National Center for Atmospheric Research, which is a major facility sponsored by the National Science Foundation under Cooperative Agreement No. 1852977.

References

Arellano, A. F. J., Kasibhatla, P. S., Giglio, L., van der Werf, G. R., & Randerson, J. T. (2004). Top-down estimates of global CO sources using MOPITT measurements. *Geophysical Research Letters*, *31*, L01104. https://doi.org/10.1029/2003GL018609

Barré, J., Gaubert, B., Arellano, A. F. J., Worden, H. M., Edwards, D. P., Deeter, M. N., et al. (2015). Assessing the impacts of assimilating IASI and MOPITT CO retrievals using CESM-CAM-chem and DART. *Journal of Geophysical Research: Atmospheres*, *120*, 10501–10529. https://doi.org/10.1002/2015JD023467

Beirle, S., Boersma, K. F., Platt, U., Lawrence, M. G., & Wagner, T. (2011). Megacity emissions and lifetimes of nitrogen oxides probed from space. *Science*, *333*(6050), 1737–1739. https://doi.org/10.1126/science.1207824

Beirle, S., Borger, C., Dörner, S., Li, A., Hu, Z., Liu, F., et al. (2019). Pinpointing nitrogen oxide emissions from space. *Science Advances*, *5*(11), eaax9800. https://doi.org/10.1126/sciadv.aax9800

Bey, I., Jacob, D. J., Yantosca, R. M., Logan, J. A., Field, B. D., Fiore, A. M., et al. (2001). Global modeling of tropospheric chemistry with assimilated meteorology: Model description and evaluation. *Journal of Geophysical Research*, *106*(D19), 23073–23095. https://doi.org/10.1029/2001JD000807

Chin, M., Rood, R. B., Lin, S.-J., Müller, J.-F., & Thompson, A. M. (2000). Atmospheric sulfur cycle simulated in the global model GOCART: Model description and global properties. *Journal of Geophysical Research*, *105*(D20), 24671–24687. https://doi.org/10.1029/2000JD900384

Crippa, M., Solazzo, E., Huang, G., Guizzardi, D., Koffi, E., Muntean, M., et al. (2020). High resolution temporal profiles in the emissions database for global atmospheric Research. *Scientific Data*, *7*(1), 121. https://doi.org/10.1038/s41597-020-0462-2

Deeter, M. N., Edwards, D. P., Francis, G. L., Gille, J. C., Mao, D., Martinez-Alonso, S., et al. (2019). Radiance-based retrieval bias mitigation for the MOPITT instrument: The version 8 product. *Atmospheric Measurement Techniques*, *12*(8), 45614580. https://doi.org/10.5194/amt-12-4561-2019

de Foy, B., & Schauer, J. J. (2019). Changes in speciated PM2.5 concentrations in Fresno, California, due to NO_x reductions and variations in diurnal emission profiles by day of week. *Element: Science of the Anthropocene*, *7*, 45. https://doi.org/10.1525/elementa.384

Ding, J., van der A, R. J., Mijling, B., Levelt, P. F., & Hao, N. (2015). NO_x emission estimates during the 2014 Youth Olympic Games in Nanjing. *Atmospheric Chemistry and Physics*, *15*(16), 9399–9412. https://doi.org/10.5194/acp-15-9399-2015

Duncan, B. N., Yoshida, Y., de Foy, B., Lamsal, L. N., Streets, D. G., Lu, Z., et al. (2013). The observed response of ozone monitoring instrument (OMI) NO_2 columns to NO_x emission controls on power plants in the United States: 2005–2011. *Atmospheric Environment*, *81*, 102–111. https://doi.org/10.1016/j.atmosenv.2013.08.068

Eastham, S. D., Long, M. S., Keller, C. A., Lundgren, E., Yantosca, R. M., Zhuang, J., et al. (2018). GEOS-chem high performance (GCHP v11-02c): A next-generation implementation of the GEOS-chem chemical transport model for massively parallel applications. *Geoscientific Model Development*, *11*(7), 2941–2953. https://doi.org/10.5194/gmd-11-2941-2018

Elguindi, N., Granier, C., Stavrakou, T., Darras, S., Bauwens, M., Cao, H., et al. (2020). Intercomparison of magnitudes and trends in anthropogenic surface emissions from bottom-up inventories, top-down estimates, and emission scenarios. *Earth's Future*, *8*(8), e2020EF001520. https://doi.org/10.1029/2020EF001520

Fioletov, V., McLinden, C. A., Griffin, D., Krotkov, N., Liu, F., & Eskes, H. (2021). Quantifying urban, industrial, and background changes in NO_2 during the COVID-19 lockdown period based on TROPOMI satellite observations. *Atmospheric Chemistry and Physics Discussions*. https://doi.org/10.5194/acp-2021-536

Fioletov, V., McLinden, C. A., Kharol, S. K., Krotkov, N. A., Li, C., Joiner, J., et al. (2017). Multi-source SO_2 emission retrievals and consistency of satellite and surface measurements with reported emissions. *Atmospheric Chemistry and Physics*, *17*(20), 12597–12616. https://doi.org/10.5194/acp-17-12597-2017

Fioletov, V., McLinden, C. A., Krotkov, N., Li, C., Joiner, J., Theys, N., et al. (2016). A global catalogue of large SO_2 sources and emissions derived from the ozone monitoring instrument. *Atmospheric Chemistry and Physics*, *16*(18), 11497–11519. https://doi.org/10.5194/acp-16-11497-2016

Fortems-Cheiney, A., Chevallier, F., Pison, I., Bousquet, P., Szopa, S., Deeter, M. N., & Clerbaux, C. (2011). Ten years of CO emissions as seen from measurements of pollution in the troposphere (MOPITT). *Journal of Geophysical Research*, *116*, D05304. https://doi.org/10.1029/2010JD014416

Gaubert, B., Arellano, A. F. Jr, Barré, J., Worden, H. M., Emmons, L. K., Tilmes, S., et al. (2016). Toward a chemical reanalysis in a coupled chemistry-climate model: An evaluation of MOPITT CO assimilation and its impact on tropospheric composition. *Journal of Geophysical Research: Atmospheres*, *121*, 7310–7343. https://doi.org/10.1002/2016JD024863

Gaubert, B., Emmons, L. K., Reader, K., Tilmes, S., Miyazaki, K., Arellano, A. F. Jr, et al. (2020). Correcting model biases of CO in East Asia: Impact on oxidant distributions during KORUS-AQ. *Atmospheric Chemistry and Physics*, *20*, 14617–14647. https://doi.org/10.5194/acp-20-14617-2020

Geng, G., Zhang, Q., Tong, D., Li, M., Zheng, Y., Wang, S., & He, K. (2017). Chemical composition of ambient PM2.5 over China and relationship to precursor emissions during 2005–2012. *Atmospheric Chemistry and Physics*, *17*(14), 9187–9203. https://doi.org/10.5194/acp-17-9187-2017

Giglio, L., Randerson, J. T., & van der Werf, G. R. (2013). Analysis of daily, monthly, and annual burned area using the fourth-generation global fire emissions database (GFED4). *Journal of Geophysical Research: Biogeosciences*, *118*, 317–328. https://doi.org/10.1002/jgrg.20042

Goldberg, D. L., Lu, Z., Streets, D. G., de Foy, B., Griffin, D., McLinden, C. A., et al. (2019). Enhanced capabilities of TROPOMI NO_2: Estimating NO_X from north American cities and power plants. *Environmental Science & Technology*, *53*(21), 12594–12601. https://doi.org/10.1021/acs.est.9b04488

Henze, D. K., Hakami, A., & Seinfeld, J. H. (2007). Development of the adjoint of GEOS-Chem. *Atmospheric Chemistry and Physics*, *7*(9), 2413–2433. https://doi.org/10.5194/acp-7-2413-2007

Henze, D. K., Seinfeld, J. H., & Shindell, D. T. (2009). Inverse modeling and mapping US air quality influences of inorganic PM2.5 precursor emissions using the adjoint of GEOS-Chem. *Atmospheric Chemistry and Physics*, *9*(16), 5877–5903. https://doi.org/10.5194/acp-9-5877-2009

Hoesly, R. M., Smith, S. J., Feng, L., Klimont, Z., Janssens-Maenhout, G., Pitkanen, T., et al. (2018). Historical (1750–2014) anthropogenic emissions of reactive gases and aerosols from the Community Emissions Data System (CEDS). *Geoscientific Model Development*, *11*(1), 369–408. https://doi.org/10.5194/gmd-11-369-2018

Jaeglé, L., Steinberger, L., Martin, R. V., & Chance, K. (2005). Global partitioning of NO_x sources using satellite observations: Relative rols of fossil fuel combustion, biomass burning and soil emissions. *Faraday Discussions*, *130*, 407–423. https://doi.org/10.1039/b502128f

Janssens-Maenhout, G., Crippa, M., Guizzardi, D., Dentener, F., Muntean, M., Pouliot, G., et al. (2015). HTAP_v2.2: A mosaic of regional and global emission grid maps for 2008 and 2010 to study hemispheric transport of air pollution. *Atmospheric Chemistry and Physics*, *15*(19), 11411–11432. https://doi.org/10.5194/acp-15-11411-2015

Jiang, Z., Jones, D. B. A., Worden, H. M., Deeter, M. N., Henze, D. K., Worden, J., et al. (2013). Impact of model errors in convective transport on CO source estimates inferred from MOPITT CO retrievals. *Journal of Geophysical Research: Atmospheres*, *118*, 2073–2083. https://doi.org/10.1002/jgrd.50216

Jiang, Z., Jones, D. B. A., Worden, H. M., & Henze, D. K. (2015). Sensitivity of top-down CO source estimates to the modeled vertical structure in atmospheric CO. *Atmospheric Chemistry and Physics*, *15*(3), 1521–1537. https://doi.org/10.5194/acp-15-1521-2015

Jiang, Z., Worden, J. R., Worden, H., Deeter, M., Jones, D. B. A., Arellano, A. F., & Henze, D. K. (2017). A 15-year record of CO emissions constrained by MOPITT CO observations. *Atmospheric Chemistry and Physics*, *17*(7), 4565–4583. https://doi.org/10.5194/acp-17-4565-2017

Kopacz, M., Jacob, D. J., Fisher, J. A., Logan, J. A., Zhang, L., Megretskaia, I. A., et al. (2010). Global estimates of CO sources with high resolution by adjoint inversion of multiple satellite datasets (MOPITT, AIRS, SCIAMACHY, TES). *Atmospheric Chemistry and Physics*, *10*(3), 855–876. https://doi.org/10.5194/acp-10-855-2010

Kopacz, M., Jacob, D. J., Henze, D. K., Heald, C. L., Streets, D. G., & Zhang, Q. (2009). Comparison of adjoint and analytical Bayesian inversion methods for constraining Asian sources of carbon monoxide using satellite (MOPITT) measurements of CO columns. *Journal of Geophysical Research*, *114*, D04305. https://doi.org/10.1029/2007JD009264

Krotkov, N. A., Lamsal, L. N., Celarier, E. A., Swartz, W. H., Marchenko, S. V., Bucsela, E. J., et al. (2017). The version 3 OMI NO_2 standard product. *Atmospheric Measurement Techniques*, *10*(9), 3133–3149. https://doi.org/10.5194/AMT-10-3133-2017

Kurokawa, J., Ohara, T., Morikawa, T., Hanayama, S., Janssens-Maenhout, G., Fukui, T., et al. (2013). Emissions of air pollutants and greenhouse gases over Asian regions during 2000–2008: Regional Emission inventory in ASia (REAS) version 2. *Atmospheric Chemistry and Physics*, *13*(21), 11019–11058. https://doi.org/10.5194/acp-13-11019-2013

Lamsal, L. N., Martin, R. V., Padmanabhan, A., van Donkelaar, A., Zhang, Q., Sioris, C. E., et al. (2011). Application of satellite observations for timely updates to global anthropogenic NO_x emission inventories. *Geophysical Research Letters*, *38*, L05810. https://doi.org/10.1029/2010GL046476

Lamsal, L. N., Martin, R. V., van Donkelaar, A., Steinbacher, M., Celarier, E. A., Bucsela, E., et al. (2008). Ground-level nitrogen dioxide concentrations inferred from the satellite-borne Ozone Monitoring Instrument. *Journal of Geophysical Research: Atmospheres*, *113*, D16308. https://doi.org/10.1029/2007JD009235

Laughner, J. L., Zare, A., & Cohen, R. C. (2016). Effects of daily meteorology on the interpretation of space-based remote sensing of NO_2. *Atmospheric Chemistry and Physics*, *16*(23), 15247–15264. https://doi.org/10.5194/acp-16-15247-2016

Lee, C., Martin, R. V., van Donkelaar, A., Lee, H., Dickerson, R. R., Hains, J. C., et al. (2011). SO_2 emissions and lifetimes: Estimates from inverse modeling using in situ and global, space-based (SCIAMACHY and OMI) observations. *Journal of Geophysical Research*, *116*, D06304. https://doi.org/10.1029/2010JD014758

Li, C., McLinden, C., Fioletov, V., Krotkov, N., Carn, S., Joiner, J., et al. (2017). India is overtaking China as the World's largest emitter of anthropogenic sulfur dioxide. *Scientific Reports*, *7*(1), 14304. https://doi.org/10.1038/s41598-017-14639-8

Li, M., Zhang, Q., Kurokawa, J. I., Woo, J. H., He, K., Lu, Z., et al. (2017). Mix: A mosaic Asian anthropogenic emission inventory under the international collaboration framework of the MICS-Asia and HTAP. *Atmospheric Chemistry and Physics*, *17*(2), 935–963. https://doi.org/10.5194/acp-17-935-2017

Liu, F., Choi, S., Li, C., Fioletov, V. E., McLinden, C. A., Joiner, J., et al. (2018). A new global anthropogenic SO_2 emission inventory for the last decade: A mosaic of satellite-derived and bottom-up emissions. *Atmospheric Chemistry and Physics*, *18*(22), 16571–16586. https://doi.org/10.5194/acp-18-16571-2018

Liu, F., Zhang, Q., van der A, R. J., Zheng, B., Tong, D., Yan, L., et al. (2016). Recent reduction in NO_x emissions over China: Synthesis of satellite observations and emission inventories. *Environmental Research Letters*, *11*(11), 114002. https://doi.org/10.1088/1748-9326/11/11/114002

Liu, H., Jacob, D. J., Bey, I., & Yantosca, R. M. (2001). Constraints from 210Pb and 7Be on wet deposition and transport in a global three-dimensional chemical tracer model driven by assimilated meteorological fields. *Journal of Geophysical Research*, *106*(D11), 12109–12128. https://doi.org/10.1029/2000JD900839

Lu, Z., Zhang, Q., & Streets, D. G. (2011). Sulfur dioxide and primary carbonaceous aerosol emissions in China and India, 1996–2010. *Atmospheric Chemistry and Physics*, *11*(18), 9839–9864. https://doi.org/10.5194/acp-11-9839-2011

Martin, R. V., Jacob, D. J., Chance, K., Kurosu, T. P., Palmer, P. I., & Evans, M. J. (2003). Global inventory of nitrogen oxide emissions constrained by space-based observations of NO_2 columns. *Journal of Geophysical Research*, *108*(D17), 4537. https://doi.org/10.1029/2003JD003453

McDuffie, E. E., Smith, S. J., O'Rourke, P., Tibrewal, K., Venkataraman, C., Marais, E. A., et al. (2020). A global anthropogenic emission inventory of atmospheric pollutants from sector- and fuel-specific sources (1970–2017): An application of the community emissions data system (CEDS). *Earth System Science Data*, *12*(4), 3413–3442. https://doi.org/10.5194/essd-12-3413-2020

McLinden, C. A., Fioletov, V., Shephard, M. W., Krotkov, N., Li, C., Martin, R. V., et al. (2016). Space-based detection of missing sulfur dioxide sources of global air pollution. *Nature Geoscience*, *9*(7), 496–500. https://doi.org/10.1038/ngeo2724

Miyazaki, K., Bowman, K., Sekiya, T., Eskes, H., Boersma, F., Worden, H., et al. (2020). Updated tropospheric chemistry reanalysis and emission estimates, TCR-2, for 2005–2018. *Earth System Science Data*, *12*(3), 2223–2259. https://doi.org/10.5194/essd-12-2223-2020

Miyazaki, K., Eskes, H., Sudo, K., Boersma, K. F., Bowman, K., & Kanaya, Y. (2017). Decadal changes in global surface NO_x emissions from multi-constituent satellite data assimilation. *Atmospheric Chemistry and Physics*, *17*(2), 807–837. https://doi.org/10.5194/acp-17-807-2017

Miyazaki, K., Eskes, H. J., & Sudo, K. (2012). Global NO_x emission estimates derived from an assimilation of OMI tropospheric NO_2 columns. *Atmospheric Chemistry and Physics*, *12*(5), 2263–2288. https://doi.org/10.5194/acp-12-2263-2012

Müller, J. F., & Stavrakou, T. (2005). Inversion of CO and NO_x emissions using the adjoint of the IMAGES model. *Atmospheric Chemistry and Physics*, *5*(5), 1157–1186. https://doi.org/10.5194/acp-5-1157-2005

Müller, J.-F., Stavrakou, T., Bauwens, M., George, M., Hurtmans, D., Coheur, P.-F., et al. (2018). Top-down CO emissions based on IASI observations and hemispheric constraints on OH levels. *Geophysical Research Letters*, *45*, 1621–1629. https://doi.org/10.1002/2017GL076697

Palmer, P. I., Jacob, D. J., Fiore, A. M., Martin, R. V., Chance, K., & Kurosu, T. P. (2003). Mapping isoprene emissions over North America using formaldehyde column observations from space. *Journal of Geophysical Research*, *108*(D6), 4180. https://doi.org/10.1029/2002JD002153

Park, R. J., Jacob, D. J., Field, B. D., Yantosca, R. M., & Chin, M. (2004). Natural and transboundary pollution influences on sulfate-nitrate-ammonium aerosols in the United States: Implications for policy. *Journal of Geophysical Research*, *109*, D15204. https://doi.org/10.1029/2003JD004473

Qu, Z., Henze, D. K., Capps, S. L., Wang, Y., Xu, X., Wang, J., & Keller, M. (2017). Monthly top-down NO_x emissions for China (2005–2012): A hybrid inversion method and trend analysis. *Journal of Geophysical Research: Atmospheres*, *122*, 4600–4625. https://doi.org/10.1002/2016JD025852

Qu, Z., Henze, D. K., Cooper, O. R., & Neu, J. L. (2020). Impacts of global NO_x inversions on NO_2 and ozone simulations. *Atmospheric Chemistry and Physics*, *20*(21), 13109–13130. https://doi.org/10.5194/acp-20-13109-2020

Qu, Z., Henze, D. K., Li, C., Theys, N., Wang, Y., Wang, J., et al. (2019). SO_2 emission estimates using OMI SO_2 retrievals for 2005–2017. *Journal of Geophysical Research: Atmospheres*, *124*, 8336–8359. https://doi.org/10.1029/2019JD030243

Qu, Z., Henze, D. K., Theys, N., Wang, J., & Wang, W. (2019). Hybrid mass balance/4D-Var Joint inversion of NO_x and SO_2 emissions in East Asia. *Journal of Geophysical Research: Atmospheres*, *124*, 8203–8224. https://doi.org/10.1029/2018JD030240

Qu, Z., Jacob, D. J., Silvern, R. F., Shah, V., Campbell, P. C., Valin, L. C., & Murray, L. T. (2021). US COVID-19 shutdown demonstrates importance of background NO_2 in inferring NO_x emissions from satellite NO_2 observations. *Geophysical Research Letters*, *48*, e2021GL092783. https://doi.org/10.1029/2021GL092783

Saikawa, E., Kim, H., Zhong, M., Avramov, A., Zhao, Y., Janssens-Maenhout, G., et al. (2017). Comparison of emissions inventories of anthropogenic air pollutants and greenhouse gases in China. *Atmospheric Chemistry and Physics*, *17*(10), 6393–6421. https://doi.org/10.5194/acp-17-6393-2017

Seinfeld, J. H., & Pandis, S. N. (2012). *Atmospheric chemistry and physics: From air pollution to climate change*. John Wiley & Sons.

Silva, S. J., & Arellano, A. F. (2017). Characterizing regional-scale combustion using satellite retrievals of CO, NO_2 and CO_2. *Remote Sensing*, *9*(7), 744. https://doi.org/10.3390/rs9070744

Silvern, R. F., Jacob, D. J., Mickley, L. J., Sulprizio, M. P., Travis, K. R., Marais, E. A., et al. (2019). Using satellite observations of tropospheric NO_2 columns to infer long-term trends in US NO_x emissions: The importance of accounting for the free tropospheric NO_2 background. *Atmospheric Chemistry and Physics*, *19*(13), 8863–8878. https://doi.org/10.5194/acp-19-8863-2019

Stibig, H. J., Achard, F., Carboni, S., Raši, R., & Miettinen, J. (2014). Change in tropical forest cover of Southeast Asia from 1990 to 2010. *Biogeosciences*, *11*(2), 247–258. https://doi.org/10.5194/bg-11-247-2014

Streets, D. G., Zhang, Q., Wang, L., He, K., Hao, J., Wu, Y., et al. (2006). Revisiting China's CO emissions after the transport and chemical evolution over the Pacific (TRACE-P) mission: Synthesis of inventories, atmospheric modeling, and observations. *Journal of Geophysical Research*, *111*, D14306. https://doi.org/10.1029/2006JD007118

Tang, W., Arellano, A. F., Gaubert, B., Miyazaki, K., & Worden, H. M. (2019). Satellite data reveal a common combustion emission pathway for major cities in China. *Atmospheric Chemistry and Physics*, *19*(7), 4269–4288. https://doi.org/10.5194/acp-19-4269-2019

Theys, N., De Smedt, I., van Gent, J., Danckaert, T., Wang, T., Hendrick, F., et al. (2015). Sulfur dioxide vertical column DOAS retrievals from the Ozone Monitoring Instrument: Global observations and comparison to ground-based and satellite data. *Journal of Geophysical Research: Atmospheres*, *120*, 2470–2491. https://doi.org/10.1002/2014JD022657

Valin, L. C., Russell, A. R., Hudman, R. C., & Cohen, R. C. (2011). Effects of model resolution on the interpretation of satellite NO_2 observations. *Atmospheric Chemistry and Physics*, *11*(22), 11647–11655. https://doi.org/10.5194/acp-11-11647-2011

Wang, Y., Jacob, D. J., & Logan, J. A. (1998). Global simulation of tropospheric O_3-NO_x-hydrocarbon chemistry: 1. Model formulation. *Journal of Geophysical Research*, *103*(D9), 10713–10725. https://doi.org/10.1029/98JD00158

Wang, Y., Wang, J., Xu, X., Henze, D. K., Wang, Y., & Qu, Z. (2016). A new approach for monthly updates of anthropogenic sulfur dioxide emissions from space: Application to China and implications for air quality forecasts. *Geophysical Research Letters*, *43*, 9931–9938. https://doi.org/10.1002/2016GL070204

Wesely, M. L. (1989). Parameterization of surface resistances to gaseous dry deposition in regional-scale numerical models. *Atmospheric Environment*, *23*(6), 1293–1304. https://doi.org/10.1016/0004-6981(89)90153-4

Worden, H. M., Deeter, M. N., Edwards, D. P., Gille, J. C., Drummond, J. R., & Nédélec, P. (2010). Observations of near-surface carbon monoxide from space using MOPITT multispectral retrievals. *Journal of Geophysical Research*, *115*, D18314. https://doi.org/10.1029/2010JD014242

Yin, Y., Chevallier, F., Ciais, P., Broquet, G., Fortems-Cheiney, A., Pison, I., & Saunois, M. (2015). Decadal trends in global CO emissions as seen by MOPITT. *Atmospheric Chemistry and Physics*, *15*(23), 13433–13451. https://doi.org/10.5194/acp-15-13433-2015

Zhang, Q., Streets, D. G., Carmichael, G. R., He, K. B., Huo, H., Kannari, A., et al. (2009). Asian emissions in 2006 for the NASA INTEX-B mission. *Atmospheric Chemistry and Physics*, *9*(14), 5131–5153. https://doi.org/10.5194/acp-9-5131-2009

Zhang, X., Jones, D. B. A., Keller, M., Walker, T. W., Jiang, Z., Henze, D. K., et al. (2019). Quantifying emissions of CO and NO_x using observations from MOPITT, OMI, TES, and OSIRIS. *Journal of Geophysical Research: Atmospheres*, *124*, 1170–1193. https://doi.org/10.1029/2018JD028670

Zhao, Y., Nielsen, C. P., Lei, Y., McElroy, M. B., & Hao, J. (2011). Quantifying the uncertainties of a bottom-up emission inventory of anthropogenic atmospheric pollutants in China. *Atmospheric Chemistry and Physics*, *11*(5), 2295–2308. https://doi.org/10.5194/acp-11-2295-2011

Zheng, B., Chevallier, F., Ciais, P., Yin, Y., Deeter, M. N., Worden, H. M., et al. (2018). Rapid decline in carbon monoxide emissions and export from East Asia between years 2005 and 2016. *Environmental Research Letters*, *13*(4), 044007. https://doi.org/10.1088/1748-9326/aab2b3

Zheng, B., Chevallier, F., Yin, Y., Ciais, P., Fortems-Cheiney, A., Deeter, M. N., et al. (2019). Global atmospheric carbon monoxide budget 2000–2017 inferred from multi-species atmospheric inversions. *Earth System Science Data*, *11*(3), 1411–1436. https://doi.org/10.5194/essd-11-1411-2019

Zheng, B., Huo, H., Zhang, Q., Yao, Z. L., Wang, X. T., Yang, X. F., et al. (2014). High-resolution mapping of vehicle emissions in China in 2008. *Atmospheric Chemistry and Physics*, *14*(18), 9787–9805. https://doi.org/10.5194/acp-14-9787-2014

Zheng, B., Zhang, Q., Geng, G., Chen, C., Shi, Q., Cui, M., et al. (2021). Changes in China's anthropogenic emissions and air quality during the COVID-19 pandemic in 2020. *Earth System Science Data*, *13*(6), 2895–2907. https://doi.org/10.5194/essd-13-2895-2021

Reference From the Supporting Information

Bucsela, E. J., Krotkov, N. A., Celarier, E. A., Lamsal, L. N., Swartz, W. H., Bhartia, P. K., et al. (2013). A new stratospheric and tropospheric NO_2 retrieval algorithm for nadir-viewing satellite instruments: Applications to OMI. *Atmospheric Measurement Techniques*, *6*(10), 2607–2626. https://doi.org/10.5194/amt-6-2607-2013